

Additives for Cycle Life Improvement of High-Voltage LNMO-Based Li-Ion Cells

Andreas Hofmann,^{*[a]} Andres Höweling,^[b] Nicole Bohn,^[b] Marcus Müller,^[b]
Joachim R. Binder,^[b] and Thomas Hanemann^[a, c]

In this empirical study, five electrolyte additives, namely, lithium bis(oxalato) borate, lithium difluoro(oxalato) borate, 1-vinyl-1,2,4-triazole, 1-vinyl imidazole and dimethyl-2,5-dioxahexane dioate are described and compared regarding their effect in LNMO/graphite cells. The additives were selected from a preliminary study of 59 potential additives. The basis electrolyte mixture is DMC/EC + 1 M LiPF₆ (LP30) for all cells. All additives are able to enhance the cycle life at room temperature and at

elevated temperatures (50 °C) significantly compared to the non-additive electrolyte blend (basis electrolyte). The cell enhancement is discussed based on the solid-electrolyte interface (SEI) and metal-ion content on anode side. The aim of the study is to suggest promising already known as well as new additives that are able to overcome the issue of rapid capacity fading of LNMO-based cells when the cells are cycled up to 4.8–5.0 V vs. Li/Li⁺, especially at higher temperatures.

1. Introduction

Electrolyte additives are able to improve the properties of Li-ion based cells significantly due to various mechanisms and principals of operation during cell formation and cycling. The most impressive effect is the improvement of the solid-electrolyte interface layer (SEI). Besides, other effects like water removal, HF catcher or manganese trapping are also inevitable, especially when considering voltage ranges above 4.5 V and sensitive electrode materials like graphite, LNMO (LiNi_{0.5}Mn_{1.5}O₄) or other Mn containing electrode materials.

The huge number of possible additives in addition with different mechanisms of individual additives aggravates the investigation of particular additive effects. Moreover, each electrode chemistry (more precisely, each electrode composition) requires highly specialized additives to provide best cycling results. Different cut-off voltages result in different additive effects (e.g. gas formation, decomposition, loss of positive cell influence). Furthermore, the combination of additives might result in not-predictable effects and cell

performances.^[1] However, a combinatorial additive approach expands the sample number dramatically (limited material and/or number of battery cycle channels). Principally, a reference electrolyte is usually working quite good, thus it is very difficult to distinguish small effects, which arise after a few hundred cycles (especially in coin cells or small pouch-bag cells). Nevertheless, these differences might determine the direction of individual electrode chemistries on the market. One might accelerate aging effects by increasing the temperature, but such an alteration might also imply other effects and is not necessarily meaningful. All these effects complicate and hamper the search for suitable additive candidates considerably.

In literature, various additives are mentioned which are able to significantly improve the cycle life, cycle performance and self-discharge.^[1–3] However, only very few studies are available which describe indeed full cells which are cycled up to or above 5 V^[4] or up to end of life (EOL; at least 80 % discharge capacity)^[5] although often electrolytes are entitled as “5 V electrolytes”.^[5,6] One new strategy is a concept to introduce compounds which are able to release additional Li⁺ ions.^[7] Nevertheless, it is quite challenging to compare different literature results with each other due to other materials used (e.g. LNMO with/without dopants, commercial or own-made LNMO, different electrode solvents), different process steps (electrode preparation, calendaring, commercial material, electrode composition) and varied cycling conditions (formation, temperature, current rates). For instance, different batches bought from the same electrode supplier resulted in completely different cycling behavior due to varying LNMO provider. Therefore, the usability of literature results, which describe only one (“new”) additive (relative to a reference), is limited as well.

The stability and ability of the additives to form suitable SEI layers often is evaluated via HOMO-LUMO calculations.^[8] It should be mentioned that these calculations are able to provide a first estimation but are not able to substitute the experimental proof, unfortunately, due to different mechanisms and effects of the various additive besides the SEI formation. HOMO-LUMO

[a] Dr. A. Hofmann, Prof. Dr. T. Hanemann
Karlsruher Institut für Technologie (KIT), Institut für Angewandte Materialien
– Werkstoffkunde (IAM-WK), Hermann-von-Helmholtz-Platz 1, 76344
Eggenstein-Leopoldshafen, Germany
Fax: +49 (0)721-608-22095
E-mail: andreas.hofmann2@kit.edu

[b] Dr. A. Höweling, Dipl.-Ing. N. Bohn, Dr. M. Müller, Dr. J. R. Binder
Karlsruher Institut für Technologie (KIT), Institut für Angewandte Materialien
– Energiespeichersysteme (IAM-ESS), Hermann-von-Helmholtz-Platz 1, 76344
Eggenstein-Leopoldshafen, Germany

[c] Prof. Dr. T. Hanemann
Universität Freiburg, Institut für Mikrosystemtechnik, Georges-Köhler-Allee
102, 79110 Freiburg, Germany



Supporting information for this article is available on the WWW under
<https://doi.org/10.1002/celc.201901120>



© 2019 The Authors. Published by Wiley-VCH Verlag GmbH & Co. KGaA.
This is an open access article under the terms of the Creative Commons
Attribution Non-Commercial License, which permits use, distribution and
reproduction in any medium, provided the original work is properly cited
and is not used for commercial purposes.

values are straightforward to calculate, but should be taken with care with respect to their physical significance.^[9] Additionally, the results are not necessarily systematic when considering additives from different molecular classes and sphere of activity.^[10] There are also other approaches, which might reveal a potential benefit in assuming additive behavior (e.g. calculating the hardness or other descriptors).^[10] However, in this case the calculations are more time consuming (e.g. calculation of neutral, anion and cation of an additive) which restricts the usability of screening a huge number of molecules. Additionally, the outcome is still limited, because also “worse” additives can have beneficial effects in a Li-ion cell (other than SEI).

In this study, an overview about five selected electrolyte additives is presented, namely lithium bis(oxalato) borate (LiBOB), lithium difluoro(oxalato) borate (LiDFOB), 1-vinyl-1,2,4-triazole (VTA), 1-vinyl imidazole (VIm) and dimethyl-2,5-dioxahexanedioate (DDD) (see Figure 1). Based on a larger evaluation study (data are shown in the supporting information), these compounds that are able to improve the cycle performance of LNMO full cells (LNMO vs. graphite) in a voltage range between 3.5–5.0 V, were obtained. The aim of the study is to investigate already known additives for lithium ion cells for their applicability in high-voltage cells and to present new additives (triazole-based and imidazole-based) to the reader, which are able to improve the lifetime of standard electrolytes. The aim is also to compare the results of the individual additives and to show possible approaches for mechanisms of action (SEI, metal ion content, layer formation) without being able to go into the exact mechanistic details.

2. Results and Discussion

In this study, electrolytes for LNMO graphite cells were investigated in detail. The cell potential as well as the half potentials of the LNMO/graphite cell with standard electrolyte ethylene carbonate/dimethyl carbonate including 1 M LiPF₆ in three electrode configuration is shown in Figure 2 at $T=25^{\circ}\text{C}$ for two cycles. This electrolyte mixture is used as basis electrolyte for all tests within the study. A corresponding dQ/dU profile is depicted in the supporting information (section 4). Distinct potential steps can be seen for graphite as well as LNMO material (Mn, Ni), as expected. Additionally it is seen that the cell pressure increases slightly during the first step.

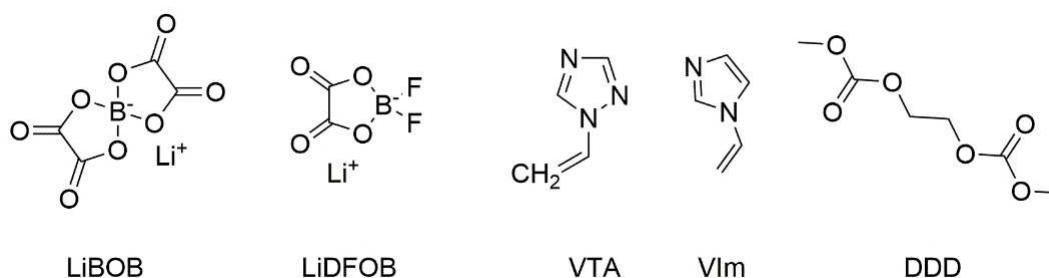


Figure 1. Overview about additives used in this study. LiBOB = lithium bis(oxalato) borate; LiDFOB = lithium difluoro(oxalato) borate; VTA = 1-vinyl-1,2,4-triazole; VIm = 1-vinyl imidazole; DDD = dimethyl-2,5-dioxahexanedioate.

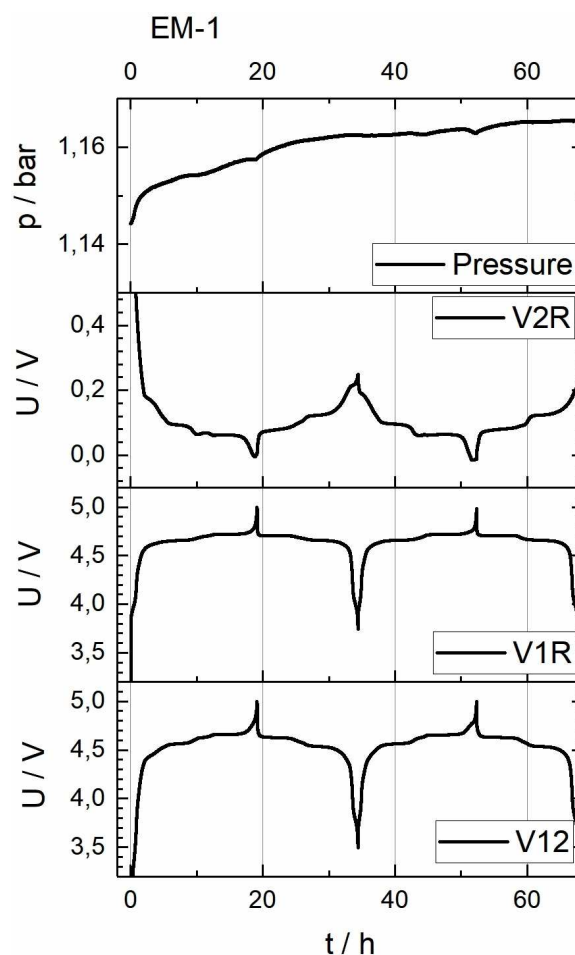


Figure 2. Potential and cell pressure within the first two cycles in 3-electrode array including WE-sense and CE sense. 1 = working electrode = LNMO; 2 = counter electrode = graphite; R = lithium metal; V = potential between two electrodes. Measured with EL-Cell PAT-press system and Zahner Zennium potentiostat. Constant current at C/15. Battery discharge capacity = 3.8 mAh. $T=25.0^{\circ}\text{C}$.

In order to find suitable additives, a screening was performed with a total of 59 additives, which were selected on the basis of existing literature and possible new SEI formers, as described in the additional information (supporting information, section 12).^[11] To accelerate the screening of the additives, the LNMO graphite cells were cycled at $T=50^{\circ}\text{C}$ (0.4 C/0.5 C). The

Table 1. Overview about cell performance at 50 °C. All coin cells (full cells, LNMO vs. graphite) are cycled between 3.5–5.0 V at 0.4 C–0.5 C (charge-discharge). In addition, results with selected additives are shown which were also tested in cell studies in this study and which have already been successfully described in the literature (possibly in other voltage limits) in LNMO or NMC cells. These additives are not further mentioned due to a selection process. A full list of tested additives is given in the supporting information.

Sample	additive ^[a]	Ref.	C ^[a] [mAh g ⁻¹]	cycle number up to 90 % C	cycle number up to 80 % C	capacity retention per cycle ^[b] [medium in %]
EM-1	–		120 ± 2	27 ± 2	70 ± 3	99.61 ± 0.10
EM-2	LiBOB	[13, 16]	120	55	108	99.81 ± 0.05
EM-3	LiDFOB	[2, 17]	123	64	122	99.79 ± 0.06
EM-4	VTA		123	43	86	99.69 ± 0.05
EM-5	VIm		123	53	108	99.75 ± 0.06
EM-6	DDD		122	38	92	99.70 ± 0.08
–	FEC	[6, 18, 19]	119	31	76	99.70 ± 0.08
–	MgTFSI ₂	[20]	112	8	33	99.53 ± 0.11
–	1,3,2-Dioxathiolane- 2,2-dioxide	[21]	121	31	72	99.66 ± 0.09
–	Succinic anhydride	[19, 22]	123	41	79	99.67 ± 0.07
–	Tris(trimethyl-silyl) borate	[23]	122	41	86	99.75 ± 0.07
–	Dimethyl phenyl phosphonite	[24]	121	26	55	99.56 ± 0.13
–	Hexamethyl disilazane	[19]	123	41	82	99.68 ± 0.07

[a] Discharge capacity at cycle number #3 at 0.4 C–0.5 C (after cell formation; cycle #1 and #2 is done with current rate of C/20–C/10) [b] Calculated based on discharge capacity values within cycle 2–70. “±”-values: standard deviation of 6 individual cells.

study showed that the individual cells can be compared well with each other up to a cycle number of ~150 before there is a clear scatter in the measurement results (Figure SI-12). All results are rated according to the cycling results until 90%, 80% and 67% state of health (SoH) in order to achieve a gradation of the additives. A detailed procedure is given in the experimental section. Selected results of this study are shown in Table 1 and compared with literature data.

The five most promising additives were selected and investigated in the study. Table 2 summarizes the composition including the five selected additives and provides results about the mixtures at $T=25^{\circ}\text{C}$. With the basis electrolyte (without additives), LNMO graphite full cells can cycled up to ~260 times

(1 C–1 C) full cycles (coin cell configuration) between 3.5–5.0 V at room temperature until 80% of the initial specific discharge capacity value is reached (SoH of 80%). The available capacity at the beginning of the 1 C/1 C cycle is shown to be in the same order of magnitude for all samples, only the sample EM-4 has a significantly lower capacity compared to the reference (EM-1) due to the increased overvoltage (see below). The discharge capacity within the first discharge cycle is $(87.4 \pm 0.7)\%$ for all samples. Capacity retention and cycle life at $T=50^{\circ}\text{C}$ are summarized in Table 1. At temperature of 50°C , the cell aging is obviously accelerated and the cell life limit (80% discharge capacity) is achieved after ~70 cycles without additives.

It is observed that the addition of all additives favors the cycling and the cycle life at room temperature as well as at 50°C . The effect is seen in case of EM-2 and EM-3 most pronounced. In Figure 3, the specific discharge capacities during cycling and the cell performance is shown at $T=25^{\circ}\text{C}$. It is found that long-term cycling is heavily dependent from many critical factors, namely the LNMO material, the LNMO electrode composition, kind of graphite electrodes, cut-off potential as well as water traces. In this sense, also the water impurity from additives is critical and must be avoided. All these factors makes it difficult to find appropriate additives with reasonable resources of time, cycling capacity and other analysis techniques (e.g., XPS, surface analysis, etc.). The performance of the cells at higher current rates ($C > 1.5$; Figure 2b) is affected due to surface layers, which are known to be formed in case of LiBOB^[12,13] and LiDFOB,^[14,15] and which stabilize the electrolytes due to its voltage drop. The cell performance correlates well with the potential drop at 5 V vs. Li/Li⁺ after starting the discharge step (Figure 4a). In this case, electrolyte EM-4 exhibits

Table 2. Overview about electrolyte mixtures and cell performance at $T=25^{\circ}\text{C}$. The reference electrolyte (EM1) is composed of EC/DMC and 1 M LiPF₆. Selected additives are added in the mixtures EM2–EM6.

Sample	additive ^[a]	c [mol kg ⁻¹]	available capacity at cycle 3 ^[b] [%]	80% capacity ^[c] [cycle number]
EM-1	–	–	85.5	255
EM-2	LiBOB	0.50 ± 0.05	85.0	610
EM-3	LiDFOB	0.50 ± 0.05	84.8	820
EM-4	VTA	0.50 ± 0.05	83.3	408
EM-5	VIm	0.50 ± 0.05	85.2	373
EM-6	DDD	0.50 ± 0.05	85.1	289

[a] LiBOB = lithium bis(oxalato) borate; LiDFOB = lithium difluoro(oxalato) borate; VTA = 1-vinyl-1,2,4-triazole; VIM = 1-Vinyl imidazole; DDD = Dimethyl-2,5-dioxahexanedioate. [b] The actual usable capacity after cell formation at 1 C–1 C (25°C) with respect to the theoretical capacity (assuming a theoretical specific capacity of 147 mAh g^{-1} of LNMO material) is listed. [c] LNMO-graphite full cells at 25°C ; provided is the cycle number when the specific discharge capacity falls below 80% of the initial discharge capacity value at the third cycle (1 C–1 C; CCCV-CC; CV-step until C/15); Hohsen coin cells configuration; $U=3.5\text{--}5.0 \text{ V}$.

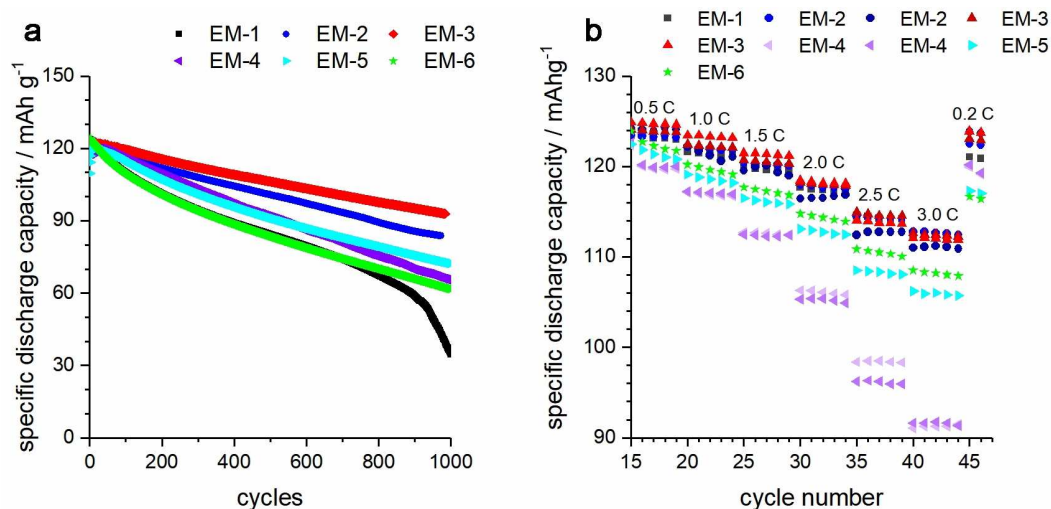


Figure 3. a) Cell cycling at 25 °C (1 C/1 C, CCCV-CC) during 1000 cycles (discharge capacity is mentioned). b) Cell cycling at 25 °C (0.4 C/0.5 C) with various current rates within the first 45 cycles.

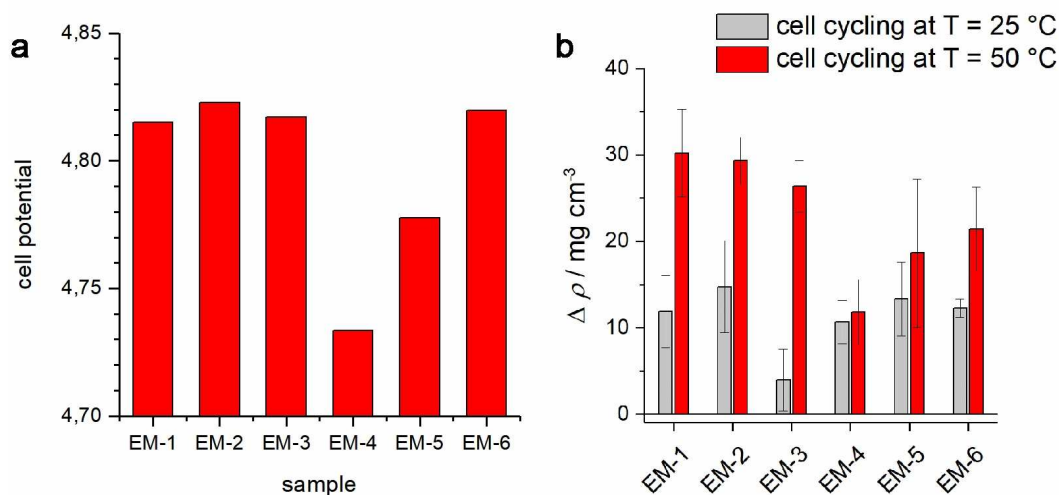


Figure 4. a) Potential drop after charging to 5.0 V within the third cycle (0.4 C CC charge rate, without CV-step). The potential was extracted after 1 s in discharge mode (C/2) (cycling at 25 °C). b) Difference in density ρ of the coin cells before and after the first 40 cycles at $T = 25$ °C and at $T = 50$ °C. The error bars illustrate the standard deviation of three individual measurements for each temperature and sample.

the largest potential drop due to thick electrode layers (see also below, SEM).

The gas formation of electrolytes,^[25] especially at high voltages, is highly critical for Li-ion cells and can hamper additives from being used in combination with selected electrode materials and cell casings, even when repeated sealing steps are included for removing gas from the formation cycles. In order to study the gas formation, the density of the cells was measured with the well-known Archimedes method directly after cell assembling and after 40 cycles (Figure 4b). At least six identical cells were analyzed for each sample. It is assumed that (1) the difference in density is caused by gas formed at higher potentials, and (2) the total mass in the cell remains constant (gas pressure increases, but the cell is not opened). In this case, the density can be correlated with the gas formation.^[26] It is observed that the gas formation is highly

temperature dependent (higher gas formation at higher temperatures) and no trend can be predicted based on previous measurements at other temperatures. Positive effects (less gas production) is observed in case of additive LiDFOB (EM-3) and VTA (EM-4). The results with additive VTA (EM-4) show almost no difference between both temperatures which might be a result of the thickness of the layer (see also below, SEM). For sample EM-3 the lowest gas formation was observed at 25 °C. The handling of the resulting gas is particularly problematic in pouch-bag cells, where the gas pressure prevents successful cell cycling. One example is the additive vinylene carbonate (VC) which is often used as an excellent SEI forming reagent. In pouch-bag cell design, the gas formation from ~4.7 V prevents the successful use of VC as an additive, although it still works well in coin test cells. The gas formation within the first two cycles of the basis electrolyte without additives were tested in

special cell holders (Figure 2 and supporting information, section 5). These measurements support the finding of the gas generation in such a way that the pressure inside the cell increases continuously. A major gas formation is observed within the first cycle. Nevertheless, afterwards the pressure increases especially during the discharge steps.

The oxidative stability of all samples is evaluated in linear sweep voltammetry (LSV) measurements against inert Pt electrodes (supporting information, section 3). Decomposition reactions can be seen for LiBOB, VTA and VIm below 3.5 V vs. Li/Li⁺ within the first polarization. LiBOB and LiDFOB exhibit a decomposition above 5 V vs. Li/Li⁺. The current density for all samples remains below 100 μAcm^{-2} up to 5.5 V at scan rate of 1 mVs^{-1} . It should be noted that these effects may vary with other electrodes significantly.^[27] All spectra reveal that the additives might be used based on their oxidative behavior in LSV measurements. HOMO-LUMO calculations are performed on DFT and MNDO basis (supporting information, section 2). Both methods are congruent with the trend that the molecules should be able to become reduced or oxidized prior to the solvents DMC/EC and LiPF₆. Cyclic voltammetry measurements were done in coin cells as well after selected cycles (supporting information, section 4 and 6). Here both main Ni redox couples can be observed between 4.3–4.7 V. With progressive cycling the CV spectra are slightly shifted to higher (charging) a lower (discharging) potentials and the absolute area under the spectra decreases due to cell aging and capacity reduction.

In Figure 5, characteristic cell efficiencies and capacity retention values are shown. It is observed that the capacity retention per cycle (i.e., how much capacity is obtained compared to the previous cycle) is almost balanced between all samples at larger cycles (cycle > 100) and exhibits a value of > 0.9992. However, at the beginning of the cycling (within the first hundred cycles) significant differences are observed between “better” additives and the reference sample. Within the first hundred cycles, the capacity retention is lower and varies significantly between 0.9987 and 0.9997. It follows from

this that the capacity values at the beginning decrease faster for worse additives and the reference sample. This correlates with a formation of a favorable SEI layer at the beginning for superior SEI forming additives, which stabilize the cell cycling and favors the capacity retention. The Coulomb efficiency values are cycling dependent. At medium cycling (at #300 at $T=25^\circ\text{C}$) Coulomb efficiency values between 0.9985 and 0.9994 are extracted for all samples. These data demonstrate an excellent performance characteristics of the electrolytes even at high voltages to 5 V. Energy efficiency values of the cells are calculated between 94–97% (supporting information, section 9).

Figure 6 shows SEM images of the graphite anode layer after cycling for 65 days. The anode sheets were washed with dimethyl carbonate to remove excessive electrolyte and salts. Larger images are also depicted in the supporting information (section 7). For comparison, cells were built that were not cyclized. These cells were disassembled after 2 weeks and the anode layer was also examined (labelled as C*). Blanc graphite sheets (C) exhibit separate graphite particles which are separated and onlay slightly covered (e.g. binder in the electrode sheet). Almost the same picture is found for the non-cycled electrode sheet (C*). In contrast, the graphite particles of all cycled cell exhibit more or less organic layers around the graphite particles. Most pronounced are the layers in case of EM-4 and EM-6. These data (EM-4) are in consistency to the cell performance (Figure 3b) and potential drop (Figure 4a) and confirm the formation of a very dense film formation for the novel triazole derivative. For electrolyte EM-5, ball-like structures are found on the particles in the cover layer which is rather an indication for no closed layer formation. The dense layer of the electrolyte EM-4 correlates well with the reduced power at higher current rates, which can be explained by an overvoltage at the solid electrolyte interface. Individual fibers in the images are from Glass fiber separators that have not been completely removed after being disassembled.

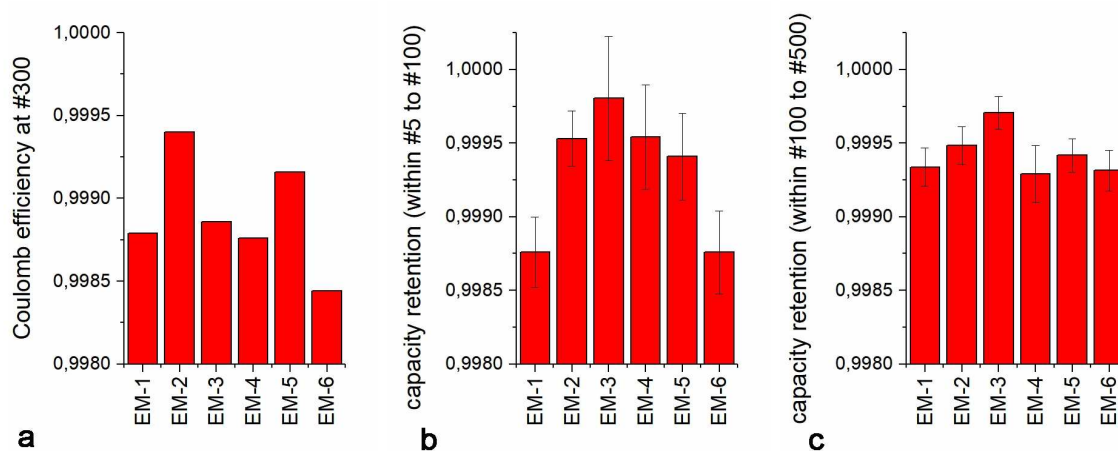


Figure 5. a) Coulombic efficiency (CE, discharge capacity related to charge capacity, Ah) at cycle 300, energy efficiency at cycle 300 (EE, discharge energy related to charge energy, Wh) and capacity retention per cycle between cycle 5–100 (b) and 100–500 (c) (CR, discharge capacity of cycle $n+1$ related to discharge capacity of cycle n) of the cells (LNMO/C) at room temperature at 1 C (CCCV-C/15)/1 C (CC). CR is provided with standard deviation of the individual cycles between #5 and #100 or #100 and #500.

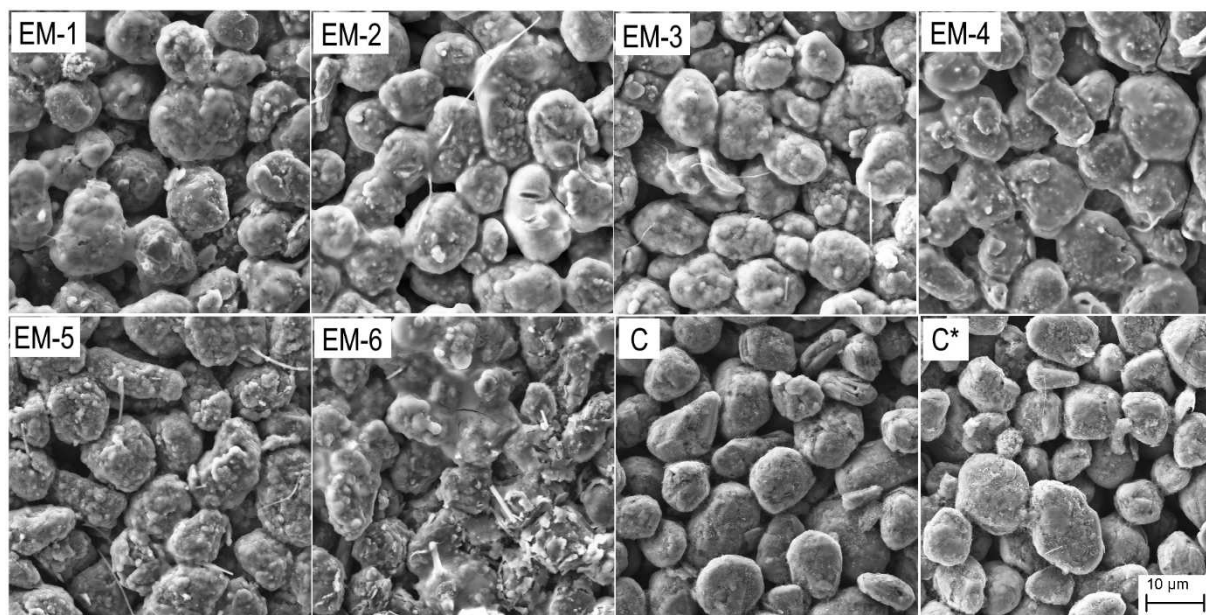


Figure 6. SEM images of anode sheets after cycling at room temperature for 65 days at 1 C/1 C (CCCV [C/15]-CC). The pure graphite (C) as well the graphite after assembling and dissembling a coin cell (C*; without cycling, the cell was stored for 14 days) are depicted in comparison. All electrodes were washed with DMC before analysis.

EDX results of the graphite electrodes are shown in Figure 7a. Results are depicted for the elements Mn as well as Ni. Other elements (C, O, P, F) are shown in supporting information (section 7). It is seen that both, Ni and Mn traces can be found on the surface of the graphite up to 4 atom-%. Interestingly, the Mn content is higher for additive-containing mixtures, which enables good cell cycling, whereas the Ni content is reduced in these cases. Apparently, this trend can be observed in the Mn-to-Ni ratio, which is highest for the electrolyte mixture EM-3 with good cycle performance. The results indicate that not only Mn plays an important role in cell

ageing, but that the Ni content also contributes to ageing in significant amount. This can be caused by catalytic processes or by favored reaction paths at the metal ions. It is already described that LiDFOB is forming an anode as well as cathode layer in the Li-ion cell.^[14,28] A high Mn-to-Ni ratio could result from a barrier of the cathode layer, especially for the Ni ions, since Mn ions with comparable concentrations were found on the anode side (EM-2, EM-3, EM-5). The oxygen content of cycled cells is significantly higher, which can be explained by the formation of solid electrolyte interfaces based on oxygen materials, e.g. ethylene carbonate, dimethyl carbonate or

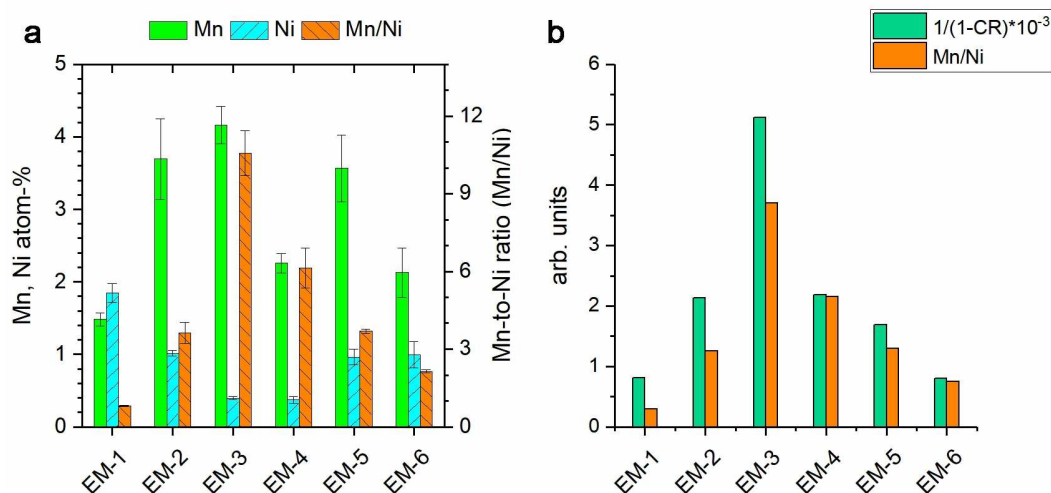


Figure 7. a) EDX results of graphite anodes after 65 d of cycling with respect to Mn and Ni concentrations. The error bars illustrate the standard deviation of three different locations onto an anode sheet. b) Correlation of the Mn-to-Ni ratio and the kinetic of the cell aging (capacity retention).

additives like oxalato-groups (supporting information). In contrast, the carbon content is reduced due to the additional layer. When Figure 5 and Figure 7a are compared, the impression arises that the Mn-to-Ni ratio correlates to a certain extent with capacity maintenance. Therefore, we have analyzed the data related to the kinetics of ageing, namely capacity retention (CR) as introduced by Höweling et al.^[4] In a first approximation, the capacity decline can be correlated with $1/(1-CR)$. In fact, this corresponds quite well to the experimentally found Mn-to-Ni ratio of the different samples (Figure 7b). The CR values of the first 100 cycles were used as a basis. The rate constant of the capacity decrease in the first estimation is proportional to the factor $CE \cdot (1-CR)/(1+CE)$.^[4] This relationship is illustrated in the Supporting Information (Figure SI-10).

AC impedance values were extracted from the cycling at the potential reversal points at 3.5 and 5.0 V. This means that the Ohmic part of the cell impedance values were recorded after each charging and discharging step by voltage drop at the maximum and minimum voltage points respectively (Figure 8). Due to the standard deviation of 1–3 Ohm between cells with same electrolyte composition (see supporting information Figure SI-11), only a general trend can be obtained: Additive LiBOB (sample EM-2) exhibits little higher overall resistance values than the other electrolyte formulation and the increase of the R_{AC} value is most pronounced in case of mixture EM-4 during cycling (especially under charging conditions, e.g. at the switching potential at 3.5 V; Figure 8/charge). Due to the fact that the performance of electrolyte EM-2 is still good (Figure 3b), the overall resistance might be effected in a different way than the Li permeability through the SEI layer. During cycling, the Ohmic part of the internal resistance increases continuously, but the increase in the internal cell resistance is larger after the discharge step than after the charging step. It should be noted that the cells are charged in CCCV (constant current + constant voltage) mode and discharged in constant current mode only. As a result, overvoltage effects become more apparent if the cells are not after-charged (or after-

discharged including a potential hold step). The difference in resistance during charging and discharging may be due to overpotentials during 1 C charge/discharge. This charge/discharge speed is already high enough to see kinetic effects and performance differences due to the solid electrolyte interface layer. Besides, it is well-known that LiBOB (electrolyte EM-2) causes overpotential effects due to SEI layer formation.^[15,29] In Figure 7 it is seen that the additive EM-3 (LiDFOB) has the most beneficial effect (lowest value of the ohmic part of internal resistance) and LiBOB (EM-2) as well as 1-vinyl-1,2,4-triazole EM-4) increase the internal resistance conspicuously. These data are in good consistency with Figure 4a.

3. Conclusion

In this study, five electrolyte additives, namely lithium bis (oxalato) borate, lithium difluoro(oxalato) borate, 1-vinyl-1,2,4-triazole, 1-vinyl imidazole and dimethyl-2,5-dioxahexanedioate were presented and investigated in LNMO graphite Li-ion full cells in a potential range between 3.5–5.0 V. The additives were selected from a preliminary study of 59 potential additives described in the Supporting Information. The 59 additives were selected on the basis of the literature and with regard to layer formation effects. Temperature-dependent cell tests (25 °C and 50 °C) showed clear differences in the additive effect, especially in ageing and gas formation. These measurements suggest that additive development should always be considered temperature-dependent in order to determine possible application effects (shortening of the service life, overvoltage effects, layer formation, gas formation). It is shown that with the additives described a clear improvement of the long-term stability at 25 °C of more than ~800 full cycles between 3.5 V and 5 V is achieved until a SoH of 80% was obtained (improvement by the factor ~3 compared to a cell without additives). Additionally, it is shown that the kinetic of cell aging correlates with the Ni-to-Mn ratio which is found on the anode in the cell. In

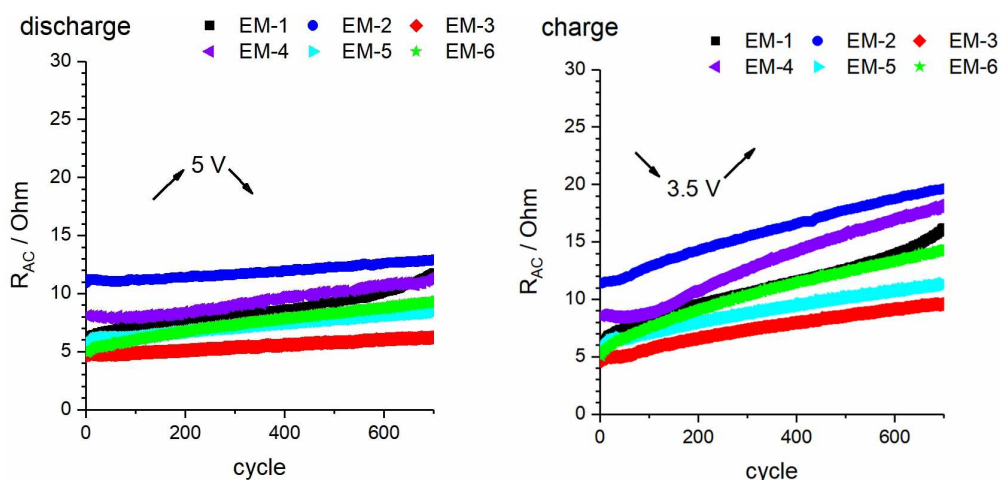


Figure 8. Ohmic part of internal resistance (R_{AC}) during charge and discharge of the cells (LNMO/C) at room temperature at 1 C (CCCV, C/15)/1 C (CC) (charge/discharge). The value was calculated based on the first measurement point of the cycle step related to the last measurement point of the previous step, namely $R_{AC} = (U_2 - U_1)/(I_2 - I_1)$. The voltage range during the measurement is outlined by the arrows and the maximum cell voltage.

comparison with 25 °C, the lifetime of the cells up to a discharge depth of 80% at 50 °C was shorter by a factor of 3.1–6.7, depending on the additive used. The most pronounced SEI growth was obtained with the additive 1-vinyl-1,2,4-triazole, visible in the voltage drop after charging and in the high internal cell resistance. The best cell results are achieved with the LiDFOB additive at current rates up to 1 C.

Experimental Section

Lithium bis(oxalato) borate (Aldrich, Art. 757136) and lithium difluoro(oxalato) borate (Aldrich, Art. 774138) were dried at 130 °C for 72 h under vacuum (vacuum oven inside glove box), whereas 1-vinyl-1,2,4-triazole (Sigma-Aldrich, Art. 95077) was dried over molecular sieve (7 d, 3 Å). After mixing with the reference electrolyte, few molecular sieve beads were added to the reference-additive-mixture (5–7 beads to 1 ml electrolyte) to avoid the contamination with water. Lithium foils (Alfa Aesar, 0.75 mm thick) were used as received. Aluminum foils (Hohsen Corp. Japan, current collector quality) and glass microfiber separators (Whatman®, GF/A with 0.26 mm and GF/B with 0.68 mm thickness) were dried at 130 °C under vacuum. Electrodes based on graphite (Custom Cells, 2.2 mAh cm⁻²) and LNMO (own-made, prepared according to reference^[4], without Ti-doping) were dried at 110 °C under vacuum for at least 48 h. The preparation of the electrolytes was performed in an argon-filled glove box (MBraun GmbH) with oxygen and water levels below 0.5 ppm. The reference electrolyte ethylene carbonate, dimethyl carbonate and 1 M LiPF₆ (electrolyte from Sigma-Aldrich, battery grade) was used as received. All electrolytes were prepared in dried Al sample vials (10 mL, Leicht & Appel GmbH).

The density of the coin cells was determined by the Archimedes method (Sartorius). The cells were weighted in air and in *iso*-propanol and the density d was calculated according to the equation $d = (m_a \cdot d_l) / (m_a - m_l)$. Here, m_a is the mass in air, m_l is the mass in *iso*-propanol and d_l is the density of the liquid at temperature T . The first measurement was done directly after the cell assembling. Thereafter, the cells were cycled for 34 cycles including a formation step. The exact procedure was following (charging-discharging): C/20–C/10 (2 cycles), 0.2 C–0.5 C (5 cycles) – 0.4 C–1 C (5 cycles) – 0.4 C–0.5 C (22 cycles) The second measurements were done at $U = 3.7$ – 3.8 V after the final discharging step. The volume of gas inside of the cells was estimated with the assumption that the mass of the formed gas can be neglected. Thus, the V_{gas} can be expressed as $V_{\text{gas}} = m_2/d_2 \cdot m_1/d_1$ (supporting information).

The cyclic voltammetry was carried out at a Zahner Zennium. Briefly, three electrode cells (EL-Cell GmbH, Hamburg, Germany) were measured in 2-electrode configuration with Li ($\varnothing = 17$ mm) (reference/counter electrode), platinum ($\varnothing = 18$ mm) (working electrode) and a Separion separator fiber ($\varnothing = 19$ mm) including electrolyte (volume: 75 μ l) in between. The potential range was set to 2.50–6.25 V vs. Li/Li⁺ and a scan speed of 1 mVs⁻¹ was used.

For electron microscopy a ZEISS Supra 55 FE-SEM was used, equipped with an EDAX EDS-system for elemental analysis. Before analysis all electrodes were washed 3 times with DMC to remove excess LiPF₆ and solvent impurities. The washing procedure was done outside of a glovebox.

For the processing of the LNMO cathodes NMP-based slurries with PVDF-binder (Solef 5130, Solvay) were coated onto 20 μ m Al foil using a continuous laboratory coater (KTF-S, Mathis) equipped with doctor-blade technology and convection drying. The composition of the LNMO sheets are: LNMO (89.3 wt.%), graphite (4 wt.%), PVDF

binder (4 wt.%) and carbon black (4 wt.%) with a coating of ~ 1.5 mAh cm⁻² (active material).

Battery tests were carried out with a cell cycler (LICCY, development of KIT, Institute of Data Processing and Electronics). The potentials reported in this work are that of the anode electrode with respect to the counter electrode. Charging and discharging cycles were conducted with current rates (C-rates) based on the capacity of the cathode material used (147 mAh g⁻¹, otherwise mentioned). All cell components were completely dried under vacuum (overnight) before they were assembled in an argon-filled glove box according to standard procedures. Additionally, all cycling was done between 3.5–5.0 V.

The coin cells were constructed with graphite (anode, C on Cu sheet, Custom Cells, 2.2 mAh cm⁻², diameter of 16.0 mm; cutted with Nogami's handheld punch), LNMO (cathode, LNMO on Al sheet, diameter of 16.0 mm, cutted with Nogami's handheld punch) and separator (Whatman QMA, diameter of 17 mm) soaked with 110 μ l electrolyte. The CR 2032 coin cells (Hohsen cases, BT innovation press) were cycled inside of a temperature chamber (Memmert, IPP30 Plus) at 50 °C (including formation process). The cycling itself was done on a LICCY cycler [REF] at 0.05 C–0.10 C (charge-discharge, CC) for two cycles and at 0.4 C–0.5 C (charge-discharge, CC) subsequently. The weight of each LNMO sheet was measured (active mass weight of 30.0 \pm 1.2 mg, standard deviation) and the current rate was calculated accordingly.

The cycling performance test was conducted at room temperature (25.0 °C) in a temperature-controlled room ($T \pm 0.5$ °C). Here, the current rate was related to the actual accessible capacity of the full cells of 130 mAh g⁻¹ (first cycle of best cells).

To determine the cell pressure, a PAT-press system from EL-Cells was used with a potentiostat from Zahner (Zahner Zennium E). Electrode sheets ($d = 18$ mm) and a QMA glass fibre separator ($d = 18$ mm) as well as 110 μ l electrolyte were used in the cell. The cell was operated in a temperature chamber at $T = 25$ °C.

All geometry optimizations were performed by using Gamess software package 16.0.^[30] HOMO-LUMO calculations were done based on a geometry/energy minimization with the MNDO method (MNDO, unrestricted open shell). Additionally, hybrid DFT calculation were carried out using the B3LYP functional. The 6-311++G(2d,p) split-valence double-zeta basis set augmented with polarization and diffuse functions was used for the calculation. Other parameters are following: restricted closed shell, POPN311, formal charges, no solvent model. HOMO and LUMO energy levels were calculated as well as the total energy of all molecules. Input files were created with the software Chem3D 16.0.1.4.

For the grade classification of the additive screening, the categories 90%, 80% and 66,7% SoH of the initial discharge capacity (third cycle at 0.5 C) were used. The quantities 108 mAh g⁻¹, 96 mAh g⁻¹ and 80 mAh g⁻¹ were calculated according to well-working cells which exhibit ~ 120 mAh g⁻¹ at the third discharge cycle (0.5 C). Cells without additives were used as reference. Based on 15 individual reference cells (RC), the following values were received for the "standard electrolyte" (medium and standard deviation, SD): 90% SoH: 27 \pm 4 cycles; 80% SoH: 70 \pm 7 cycles; 67% SoH: 136 \pm 12 cycles. All cells were cycled at 50 °C between 3.5–5.0 V (both, charging and discharging) at 0.4 C/0.5 C. Following gradation is used: "+++": at least better than +10% of best RC performance in two categories; "++": at least better than RC performance including positive SD in two categories; "+": at least better than RC medium performance in two categories; "o": at least equal than RC medium performance including negative SD in two categories; "-": worse than others. All numbers are taken from the best working individual cell at 50 °C. All capacity values are provided as discharge

capacity. More details as well as the whole list of additive results can be found in supporting information (section 10).

Acknowledgements

This work contributes to the research performed at CELEST (Center for Electrochemical Energy Storage Ulm-Karlsruhe).

Conflict of Interest

The authors declare no conflict of interest.

Keywords: LNMO · electrolytes · additives · Li-ion cell · electrochemistry · energy conversion

- [1] Q. Wang, L. Feng, J. Sun, *Energies* **2016**, *9*, 424.
- [2] H. Zhou, B. Liu, D. Xiao, C. Yin, J. Li, *J. Mater. Sci. Mater. Electron.* **2019**, *30*, 5098–5108.
- [3] a) T. Yang, H. Zeng, W. Wang, X. Zhao, W. Fan, C. Wang, X. Zuo, R. Zeng, J. Nan, *J. Mater. Chem. A* **2019**, *7*, 8292–8301; b) T. J. Lee, J. Soon, S. Chae, J. H. Ryu, S. M. Oh, *ACS Appl. Mater. Interfaces* **2019**, *11*, 11306–11316; c) H. Rong, M. Xu, B. Xie, H. Lin, Y. Zhu, X. Zheng, W. Huang, Y. Liao, L. Xing, W. Li, *J. Power Sources* **2016**, *329*, 586–593; d) M. Ershadi, M. Javanbakht, S. H. R. Beheshti, B. Mosallanejad, Z. Kiaei, *Anal. Bioanal. Electrochem.* **2018**, *10*, 1629–1653; e) X. Xu, S. Deng, H. Wang, J. Liu, H. Yan, *Nano-Micro Lett.* **2017**, *9*; f) H. Zhang, H. Zhao, M. A. Khan, W. Zou, J. Xu, L. Zhang, J. Zhang, *J. Mater. Chem. A* **2018**, *6*, 20564–20620; g) T. Zhang, E. Paillard, *Front. Chem. Sci. Eng.* **2018**, *12*, 577–591; h) H. Zhao, X. Yu, J. Li, B. Li, H. Shao, L. Li, Y. Deng, *J. Mater. Chem. A* **2019**, *7*, 8700–8722.
- [4] A. Höweling, S. Glatthaar, D. Nötzel, J. R. Binder, *J. Power Sources* **2015**, *274*, 1267–1275.
- [5] A. von Cresce, K. Xu, *J. Electrochem. Soc.* **2011**, *158*, A337–A342.
- [6] Y. Xu, J. Liu, L. Zhou, L. Zeng, Z. Yang, *J. Electroanal. Chem.* **2017**, *791*, 109–116.
- [7] S. Solchenbach, M. Wetjen, D. Pritzl, K. U. Schwenke, H. A. Gasteiger, *J. Electrochem. Soc.* **2018**, *165*, A512–A524.
- [8] a) Y. Okamoto, Y. Kubo, *ACS Omega* **2018**, *3*, 7868–7874; b) M. Yoshio, H. Nakamura, N. Dimov in *Lithium Ion Rechargeable Batteries, 1st ed.*, (Eds.: K. Ozawa), Wiley-VCH, Weinheim, **2009**, pp. 163–177.
- [9] G. Zhang, C. B. Musgrave, *J. Phys. Chem. A* **2007**, *111*, 1554–1561.
- [10] P. Jankowski, W. Wiczorek, P. Johansson, *J. Mol. Model.* **2017**, *23*, 6.
- [11] K. Abe in *Electrolytes for Lithium and Lithium-Ion Batteries, 1st ed.*, Vol. 58 (Eds.: T. R. Jow, K. Xu, O. Borodin, M. Ue) Springer, New York, **2014**, pp. 167–208.
- [12] a) K. Xu, S. Zhang, T. R. Jow, *Electrochem. Solid-State Lett.* **2003**, *6*, A117–A120; b) G. V. Zhuang, K. Xu, T. R. Jow, J. P. N. Ross, *Electrochem. Solid-State Lett.* **2004**, *7*, A224–A227.
- [13] N. P. W. Pieczonka, L. Yang, M. P. Balogh, B. R. Powell, K. Chemelewski, A. Manthiram, S. A. Krachkovskiy, G. R. Goward, M. Liu, J.-H. Kim, *J. Phys. Chem. C* **2013**, *117*, 22603–22612.
- [14] M. Xu, L. Zhou, L. Hao, L. Xing, W. Li, B. L. Lucht, *J. Power Sources* **2011**, *196*, 6794–6801.
- [15] I. A. Shkrob, Y. Zhu, T. W. Marin, D. P. Abraham, *J. Phys. Chem. C* **2013**, *117*, 23750–23756.
- [16] K. Xu, S. Zhang, T. R. Jow, W. Xu, C. A. Angell, *Electrochem. Solid-State Lett.* **2002**, *5*, A26–A29.
- [17] L. Dong, F. Liang, D. Wang, C. Zhu, J. Liu, D. Gui, C. Li, *Electrochim. Acta* **2018**, *270*, 426–433.
- [18] L. Wang, S. Liu, K. Zhao, J. Li, Y. Yang, G. Jia, *Ionics* **2018**, *24*, 3337–3346.
- [19] S. Ostermeyer, Conference Presentation, *Advanced Battery Power*, Aachen, **2017**.
- [20] R. Wagner, V. Kraft, B. Streipert, J. Kasnatscheew, D. R. Gallus, M. Amereller, M. Korth, I. Cekic-Laskovic, M. Winter, *Electrochim. Acta* **2017**, *228*, 9–17.
- [21] J. Xia, N. N. Sinha, L. P. Chen, J. R. Dahn, *J. Electrochem. Soc.* **2014**, *161*, A264–A274.
- [22] V. Tarnopolskiy, J. Kalhoff, M. Nádherná, D. Bresser, L. Picard, F. Fabre, M. Rey, S. Passerini, *J. Power Sources* **2013**, *236*, 39–46.
- [23] Z. Chen, C. Wang, L. Xing, X. Wang, W. Tu, Y. Zhu, W. Li, *Electrochim. Acta* **2017**, *249*, 353–359.
- [24] S. Mai, M. Xu, X. Liao, L. Xing, W. Li, *J. Power Sources* **2015**, *273*, 816–822.
- [25] a) R. Petibon, J. Harlow, D. B. Le, J. R. Dahn, *Electrochim. Acta* **2015**, *154*, 227–234; b) D. S. Hall, J. Li, K. Lin, N. Stakheiko, J. Baltazar, J. R. Dahn, *J. Electrochem. Soc.* **2019**, *166*, A793–A801.
- [26] a) J. Xia, R. Petibon, D. Xiong, L. Ma, J. R. Dahn, *J. Power Sources* **2016**, *328*, 124–135; b) D. J. Xiong, L. D. Ellis, R. Petibon, T. Hynes, Q. Q. Liu, J. R. Dahn, *J. Electrochem. Soc.* **2016**, *164*, A340–A347.
- [27] A. Hofmann, F. Werth, A. Höweling, T. Hanemann, *ECS Electrochem. Lett.* **2015**, *4*, A141–A144.
- [28] B. Deng, D. Sun, Q. Wan, H. Wang, T. Chen, X. Li, M. Qu, G. Peng, *Acta Chim. Sin.* **2018**, *76*, 259.
- [29] a) B. S. Parimalam, B. L. Lucht, *J. Electrochem. Soc.* **2018**, *165*, A251–A255; b) S. Wang, W. Qiu, T. Li, B. Yu, H. Zhao, *Int. J. Electrochem. Sci.* **2006**, *1*, 250–257; c) K. Xu, S. Zhang, T. R. Jow, *Electrochem. Solid-State Lett.* **2005**, *8*, A365–A368; d) K. Xu, S. S. Zhang, U. Lee, J. L. Allen, T. R. Jow, *J. Power Sources* **2005**, *146*, 79–85.
- [30] a) M. W. Schmidt, K. K. Baldrige, J. A. Boatz, S. T. Elbert, M. S. Gordon, J. H. Jensen, S. Koseki, N. Matsunaga, K. A. Nguyen, S. Su, T. A. Windus, M. Dupuis, J. A. Montgomery, *J. Comput. Chem.* **1993**, *14*, 1347–1363; b) M. S. Gordon, M. W. Schmidt in *Theory and Applications of Computational Chemistry: the first forty years, 1st ed.* (Eds.: C. E. Dykstra, G. Frenking, K. S. Kim, G. E. Scuseria), Elsevier, Amsterdam, **2005**, pp. 1167–1189.

Manuscript received: July 5, 2019

Revised manuscript received: September 4, 2019